CHEMISTRY
A EUROPEAN JOURNAL

DOI: 10.1002/chem.200800259

A Closer Look: Magnetic Behavior of a Three-Dimensional Cyanometalate Coordination Polymer Dominated by a Trace Amount of Nanoparticle Impurity

Julie Lefebvre,[a] Simon Trudel,[a, b] Ross H. Hill,[a, b] and Daniel B. Leznoff*[a]

Abstract: The structure and properties of the K{Ni[Au(CN)$_2$]$_3$} coordination polymer, prepared as a powder at room temperature and recrystallized hydrothermally, are reported. The structure of K{Ni[Au(CN)$_2$]$_3$} contains triply-interpenetrated Prussian Blue type pseudo-cubic arrays assembled from the alternation of octahedral Ni^{II} centers and [Au(CN)$_2$]$^-$ bridging units. SQUID magnetometry studies have shown that K{Ni[Au(CN)$_2$]$_3$} displays typical paramagnetic behavior for isolated Ni^{II} centers down to 1.8 K. However, the magnetic behavior of the samples prepared under hydrothermal conditions suggests a superparamagnetic signature superimposed onto a paramagnetic background. After investigating the samples by transmission electron microscopy, it was determined that, in addition to K{Ni[Au(CN)$_2$]$_3$}, the high-temperature (125, 135, and 165 °C) aqueous reaction of Ni(NO$_3$)$_2$·6 H$_2$O with KAu(CN)$_2$ also led to the formation of nanoparticles of NiO and Au as minor side products, and that these dominated the magnetic behavior. Nanoparticles of various sizes and shapes were observed, depending on the reaction conditions. Samples containing nanoparticles were found to be superparamagnetic, exhibiting blocking temperatures of ≈17–22 K, consistent with the behavior expected for NiO nanoparticles. These results illustrate the extreme care that must be taken when examining the physical properties of apparently analytically pure materials prepared by hydrothermal methods.

Keywords: coordination polymers · cyanometalates · hydrothermal synthesis · magnetic properties · nanomaterials

Introduction

In the last two decades, the field of coordination polymers has attracted a great deal of attention due to the promise of generating materials with specific physical properties based on the chosen building blocks.[1,2] Porous materials have been developed for gas storage applications,[3] while vapochromic coordination polymers[4,5] are promising sensing materials. Coordination polymers that exhibit nonlinear optical properties (NLO),[6,7] birefringence,[8,9] luminescence,[6,10] and combined multiple functions[11] have been important research targets within the coordination polymer realm. The investigation of new and unusual magnetic properties especially stands out as a focus of study in this area.[12,13] In particular, since the discovery of magnetic ordering in Prussian Blue, Fe$_4^{III}$[Fe^{II}(CN)$_6$]$_3$·14 H$_2$O, at 5.6 K,[14] a substantial amount of research has targeted cyanometalate coordination polymers.[12,15] Some Prussian Blue analogues have been found to become magnetically ordered at temperatures as high as 372 and 376 K.[16] Other cyanometalate coordination polymers have been found to exhibit photoinduced magnetic properties[17] or room temperature hysteretic spin transition behavior.[18]

Although the majority of coordination polymers are usually synthesized at room temperature, the simple mixing of precursor solutions often does not yield single crystals but rather generates microcrystalline powders. As the physical properties of a coordination polymer in the solid-state are expected to be a consequence of its structure, being able to determine the three-dimensional (3D) arrangement is a key step in understanding the structure–property relationships. Given this importance, the crystallization conditions are

---

[a] Dr. J. Lefebvre, Dr. S. Trudel, Prof. R. H. Hill, Prof. D. B. Leznoff
Department of Chemistry, Simon Fraser University
8888 University Drive
Burnaby BC, V5A 1S6 (Canada)
Fax: (+1) 778-782-3765
E-mail: dleznoff@sfu.ca

[b] Dr. S. Trudel, Prof. R. H. Hill
4D LABS, Simon Fraser University
8888 University Drive
Burnaby BC, V5A 1S6 (Canada)

Supporting information for this article is available on the WWW under http://dx.doi.org/10.1002/chem.200800259.

often modified to favour the formation of single crystals suitable for structure determination.[19] For example, different crystal growth techniques, such as slow evaporation of solvents, slow diffusion of reagents through H-shaped tubes and gels,[20] electrocrystallization,[21] and hydrothermal or solvothermal reactions,[22] are often used to obtain crystals suitable for X-ray crystallography. When using these modified synthesis conditions, care must be taken as different products or polymorphs may also be formed.[2,23]

The term solvothermal applies to solution reactions carried out at temperatures beyond the normal boiling point of the solvent, while remaining in the liquid phase. Such conditions can be achieved in a sealed and rigid vessel. When water is used as the solvent, the term “hydrothermal” is applied. Hydrothermal reactions are usually carried out between 100 and 250 °C.[24] Hydro- and solvothermal reactions are widely used to prepare different types of materials,[25] including zeolites,[26] inorganic solids,[27] hybrid organic–inorganic materials,[28] molecular clusters,[24] and metal oxide nanostructures.[29] Such reaction conditions allow one to: 1) recrystallize materials that are not soluble under ambient conditions; 2) increase the reactivity of inert building blocks; 3) encourage the formation of thermodynamic or other metastable products; and 4) generate unique solid materials by the in situ hydrothermal synthesis of unusual ligands in the presence of metals.[30] However, despite these advantages, the conditions of hydrothermal reactions can induce decomposition of some building blocks and allow side reactions to occur.

As part of our studies on d^{10}-cyanometalate polymers,[4,9,31,32] while investigating the physical properties of the new Prussian Blue analogue $K\{Ni[Au(CN)_2]_3\}$, prepared at room temperature as a powder or crystallized hydrothermally at temperatures ranging from 125 to 165 °C, we discovered some discrepancies in its magnetic behavior. Upon examination by electron microscopy, small amounts of nanoparticle impurities were found in the samples that had been prepared hydrothermally. Along with the properties of $K\{Ni[Au(CN)_2]_3\}$, we report herein the chemical and magnetic properties of the nanoparticle impurities, as determined through transmission electron microscopy and SQUID magnetometry studies, and the impact these have on the magnetic properties observed for the bulk samples. This cautionary narrative serves to illustrate the important lesson that great care must be taken when studying hydrothermally prepared samples to ensure that the observed physical properties are indeed attributable to the product of interest.

Results

Synthesis: The room temperature reaction of $Ni(NO_3)_2{\cdot}6H_2O$ with four equivalents of $KAu(CN)_2$ in water afforded an immediate green precipitate, which converted into a blue precipitate after several days of being stirred in the mother liquor. The FTIR spectrum, powder X-ray diffractogram, and elemental analysis of the initial green powder obtained in this reaction were indistinguishable from those of the previously reported $Ni(\mu\text{-}OH_2)_2[Au(CN)_2]_2$ coordination polymer.[32]

The FTIR spectrum of the blue powder showed only one band attributable to a cyanide vibration (2170 cm^{-1}). No hydrogen was detected by elemental analysis and the chemical composition was found to be consistent with $K\{Ni[Au(CN)_2]_3\}$. This sample (blue powder) prepared at room temperature is referred to herein as sample **RT**.

FTIR spectroscopy is an invaluable tool for studying cyanometalate coordination polymers, as the frequency corresponding to the vibration of a cyanide group is very sensitive to the environment of this group.[33] The presence of only one cyanide vibration mode observed at 2170 cm^{-1} suggests that all of the cyanide groups are in an identical environment, most likely coordinated to the Ni^{II} centers through the nitrogen atom.

Crystals suitable for single-crystal X-ray diffraction analysis could not be obtained from the blue powder by slow-diffusion methods at room temperature. In order to obtain larger single crystals, the reaction of $Ni(NO_3)_2{\cdot}6H_2O$ with $KAu(CN)_2$ was carried out under hydrothermal conditions (125 °C) with a slow cooling rate. This afforded a mixture of a pale-blue powder and dark-blue hexagonal-shaped crystals. This sample prepared at 125 °C is referred to herein as **H-125**.

The FTIR spectrum of **H-125** showed the same peak in the cyanide vibration region as the FTIR spectrum of the blue **RT** product. The elemental analysis results were also consistent with the product **H-125** being $K\{Ni[Au(CN)_2]_3\}$. In addition, the powder X-ray diffractograms of **RT** and **H-125** were found to be superimposable. Thus, the two synthetic routes afforded the same $K\{Ni[Au(CN)_2]_3\}$ product, with the same three-dimensional arrangement of building blocks.

Structure: From the X-ray diffraction data of a dark-blue hexagonal crystal obtained from the **H-125** sample, the structure of $K\{Ni[Au(CN)_2]_3\}$ was determined. The same structural motif, in which octahedral Ni^{II} centers are bridged in all three directions by $[Au(CN)_2]^-$ units to form a cubic-type Prussian Blue-like array (Figure S1, Table S1), has previously been observed in other coordination polymers of similar composition, namely $K\{Co[Au(CN)_2]_3\}$,[34] $K\{Fe[Au(CN)_2]_3\}$,[35] and $K\{Mn[Ag(CN)_2]_3\}$.[36] The powder X-ray diffractogram predicted for this structure is superimposable on those obtained experimentally from the bulk samples **RT** and **H-125**.

Magnetic behavior of $K\{Ni[Au(CN)_2]_3\}$: The magnetization of the $K\{Ni[Au(CN)_2]_3\}$ sample **RT** was measured upon cooling from 300 K to 1.8 K in a 1 kOe applied DC field. The effective magnetic moment was determined to be 3.1 μ_B at 300 K, and remained almost constant down to 10 K (Figure 1). Below this temperature, a slight decrease to 2.86 μ_B at 1.8 K was observed.

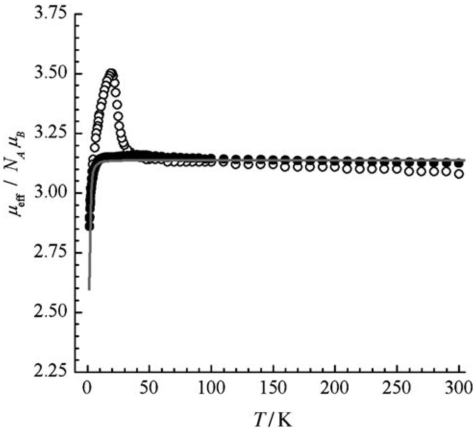

Figure 1. Temperature dependence of the effective magnetic moment for the K{Ni[Au(CN)$_2$]$_3$} samples **RT** (●) and **H-125** (○). The solid line represents the best fit for sample **RT** to the zero-field splitting equation [Equations (S1)–(S4)].

This behavior is consistent with mostly isolated Ni^{II} centers. The data can be fitted to an equation for the zero-field splitting of isolated $S=1$ centers[37] with a D value of 2.32(3) cm^{-1} and a g value of 2.22(1) (Figure 1, Figure S2, and Equations S1–S4). These values are comparable to those obtained for isolated Ni^{II} systems,[37] and also to those for the related 3D systems nBu$_4$N{Ni[Au(CN)$_2$]$_3$} and PPN{Ni[Au(CN)$_2$]$_3$} (PPN = bis(triphenylphosphoranylidene)ammonium), which display small D values and minimal coupling.[38] This indicates that, despite the 3D nature of K{Ni[Au(CN)$_2$]$_3$} (**RT**), no spontaneous magnetic ordering occurs and, at best, only weak interactions between the Ni^{II} centers are present.

The temperature dependence of the magnetization of K{Ni[Au(CN)$_2$]$_3$} (**RT**), measured upon warming (in a 10 Oe field) after being cooled in the absence (zero-field cooled (ZFC), Figure 2) or the presence (field cooled, FC) of an applied magnetic field, shows a continuous decrease, irrespective of the cooling conditions. The two curves (ZFC and FC) are superimposable. This behavior is also consistent with Curie–Weiss paramagnetism.

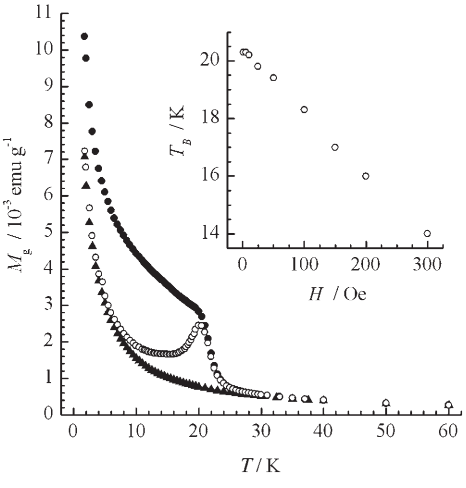

Figure 2. ZFC measurements for the K{Ni[Au(CN)$_2$]$_3$} sample **RT** (▲), and FC (●) and ZFC (○) measurements for sample **H-125** under an external field of 10 Oe. Inset: Field dependence of T_B for sample **H-125**.

The same experiments were performed on the **H-125** K{Ni[Au(CN)$_2$]$_3$} sample. The effective magnetic moment was found to be essentially constant between 300 K and 60 K (3.08–3.14 μ_B). In this case, however, an increase to a maximum value of 3.50 μ_B at 20 K was observed, followed by a decrease to 2.90 μ_B at 2.0 K (Figure 1). In the ZFC measurements performed on the **H-125** sample (Figure 2), as the temperature was increased from 1.8 K to 10 K, a decrease in the magnetization, similar to that observed for the **RT** sample, was observed. In contrast, however, above 10 K, the magnetization increased and a maximum was reached at a temperature of 20 K, referred to as T_B (see below for more explanation). Upon further warming, the magnetization decreased and, above 30 K, followed that of the ZFC and FC measurements for the **RT** sample. When ZFC measurements were performed under different external fields, the position and shape of the maximum varied from a sharp peak at 20.5 K when measured in a field of 1 Oe to a broader peak at 14 K in a field of 300 Oe (inset in Figure 2; Figure S3). The corresponding FC measurements showed an initial decrease in the magnetization, albeit a slower decrease, and then the data rejoined the ZFC curve at the temperature at which a maximum was observed in the ZFC curve for the **H-125** sample (Figure 2). On increasing the temperature further, the FC curve was seen to track the ZFC curve. As will be discussed below, this behavior is suggestive of a superparamagnetic signature superimposed onto a paramagnetic background.

Clearly, despite the spectroscopic, analytical, and diffraction data seemingly indicating that the two samples are pure and identical, the low-temperature magnetic behaviors are different, with the **H-125** system showing indications of some form of magnetic ordering or blocking (see below).[39] This magnetic behavior was consistently observed for every sample prepared under these conditions.

Transmission electron microscopy (TEM) of the K{Ni[Au(CN)$_2$]$_3$} samples: Sample **H-125** was investigated by TEM. The most obvious features observed were hexagonal crystals tens to hundreds of microns in size. Upon higher magnification and careful inspection, ensembles of particles with dimensions in the range of approximately 2–10 nm (see histogram, Figure S5) were observed (Figure 3A). The shapes of the nanocrystals ranged from spherical to oblate, with some having more convoluted morphologies.

The selected-area electron diffraction (SAED) pattern of these nanoparticles was recorded and is shown in the inset in Figure 3A. Rings can clearly be observed in the diffractogram, suggesting that the inspected area contains a randomly oriented, crystalline material. The observed electron diffraction pattern does not match the pattern that would be expected from the trigonal structure of K{Ni[Au(CN)$_2$]$_3$} as determined by single-crystal X-ray diffraction analysis. The

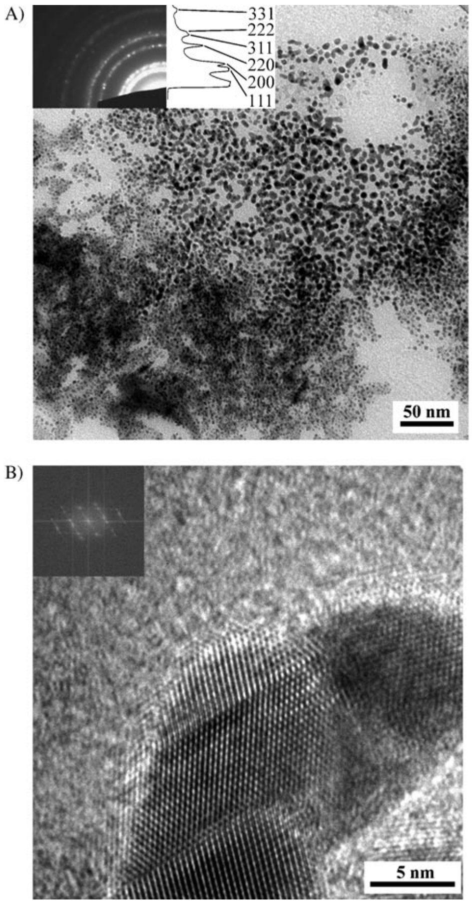

Figure 3. A) Bright-field transmission electron microscopy image of nanoparticles present in the **H-125** sample of K{Ni[Au(CN)$_2$]$_3$}. Scale bar = 50 nm. The inset shows the selected-area electron diffraction pattern of the area shown in the micrograph. The rings are indexed to *hkl* values for an *fcc* structure. B) High-resolution transmission electron microscopy image. Scale bar = 5 nm. The inset shows the fast Fourier transform of sections of the micrograph.

electron diffraction pattern readily indexes to a face-centred cubic (*fcc*) structure; the rings were assigned *hkl* values corresponding to reflections due to the (111), (200), (220), (311), (222), and (331) *fcc* planes.

A representative image of the particles observed in the **H-125** sample under high magnification is presented in Figure 3B. Under phase contrast conditions, lattice fringes can clearly be observed.

When the **RT** sample was investigated by TEM, hexagonal-shaped, micron-sized particles could be observed, as in the case of the **H-125** sample. However, despite extensive investigation, no nanoparticles could be found in the **RT** sample. Electron diffraction analysis of the large hexagonal crystals showed that they were single crystals, rather than agglomerates of nanocrystals. No SAED diffractogram arising from a collection of *fcc*-structured crystals was observed from any area of the **RT** sample.

Elemental analysis of each sample was carried out by means of energy-dispersive X-ray spectroscopy (EDXS). Figure 4A shows a high-angle annular dark-field STEM image of a representative area. Figure 4B shows the EDXS spectra of the selected areas indicated in Figure 4A. Elemental analysis of the larger hexagonal crystals showed the presence of all of the constituent elements of the K{Ni[Au(CN)$_2$]$_3$} coordination polymer, including clear signals for nitrogen and potassium (Figure 4B, spectrum ii). This is consistent with the probed region being K{Ni[Au(CN)$_2$]$_3$}. Signals for copper, beryllium, and silicon are artefacts, and are attributed to the TEM grid, its holder, and the EDXS detector, respectively. These signals were also observed in all subsequent EDXS spectra presented.

The EDXS spectrum of a region consisting of the nanoparticulate crystals was rich in gold, nickel, and oxygen, but no significant amount of nitrogen was observed, and no X-ray line due to potassium was present (Figure 4B, spectrum i). This strongly suggests that the composition of the nanoparticles differs from that of the larger, coordination polymer crystals. In all areas, a strong signal due to the presence of carbon could be observed. It is, however, impossible to differentiate between carbon from the sample and that from the supporting grid. The oxygen line may also have been due to the supporting grid (Figure 4B, spectrum iii). However, the intensity of the oxygen line (with respect to carbon) in spectrum i is much higher (by a factor of ≈2.5)

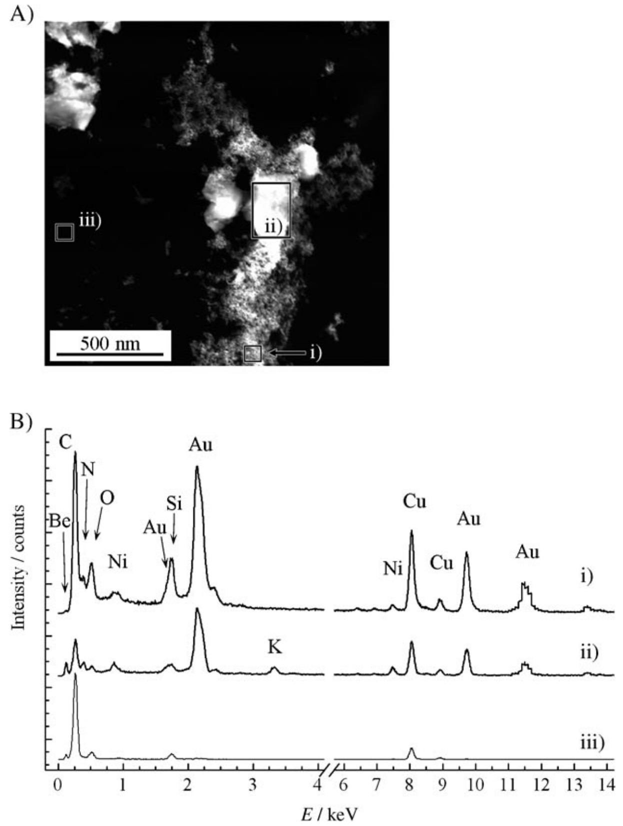

Figure 4. A) High-angle annular dark-field scanning transmission electron microscopy image of the **H-125** sample. Scale bar = 500 nm. B) Energy-dispersive X-ray spectra (EDXS) for the areas highlighted in A, showing a region containing: nanoparticles (spectrum i), K{Ni[Au(CN)$_2$]$_3$} crystals (spectrum ii), and the carbon-coated copper grid (spectrum iii).

than the oxygen:carbon line intensities in spectrum iii. Even though this is not definitive, it suggests that a significant portion of the oxygen signal in spectrum i arises from the sample. Hence, the elemental analysis of the **H-125** sample by EDXS suggests that the nanoparticles are composed of gold, nickel, and oxygen, or mixtures of these elements.

To further investigate the nanoparticle side product present in the **H-125** samples, the reaction conditions were modified. The temperature and the time for which the mixture was kept at above 125 °C were increased in an attempt to increase the yield of nanoparticles, as described below.

Sample prepared at 165 °C (H-165): A hydrothermal reaction using the same quantities of reagents was also carried out at 165 °C. A large amount of red-brown powder was obtained along with the dark-blue crystals. The bulk product is referred to herein as **H-165**.

ZFC and FC magnetization experiments were performed on sample **H-165**. Magnetic behavior qualitatively similar to that of **H-125** was observed (Figure 5). However, the maximum in magnetization attained a larger value as the maximum temperature of the reaction was increased, going from 0.245×10^{-2} emu g^{-1} for **H-125** to 8.61×10^{-2} emu g^{-1} for **H-165**. Sample **H-165** exhibited a primary maximum in magnetization at 22.75 K (compared to 20 K for sample **H-125**) and, in addition, a shoulder or a second, lesser maximum at approximately 17 K was also observed. The increase in magnetization below 5 K could be a paramagnetic tail, attributable to the $K\{Ni[Au(CN)_2]_3\}$ coordination polymer present in the samples. Magnetization versus field loops were measured at temperatures of 300, 100, 50, and 2 K (Figure S6). Above 50 K, the magnetization loops are anhysteretic and typical of paramagnetic behavior. At 2 K, the loop does not retrace itself upon field reversal. The width of the hysteretic loop is ≈25 Oe.

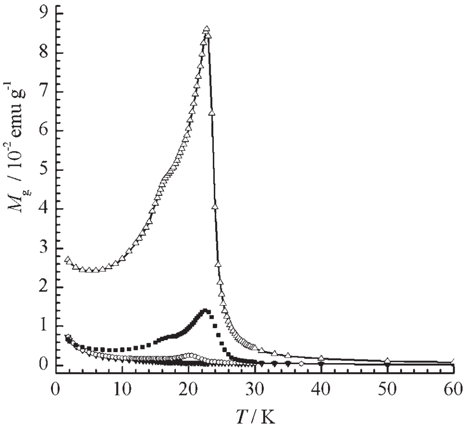

Figure 5. Comparison of the ZFC magnetic behaviors of samples **RT** (▼), **H-125** (○), **H-135** (■), and **H-165** (△). Lines are guides for the eyes.

When investigated by STEM, sample **H-165** showed different features to those observed for the **H-125** sample. Images of the red-brown powder from the **H-165** sample showed much larger particles (200–300 nm), along with filament-like particles (Figure 6A). The presence of a few smaller particles (of a few nanometres in diameter) was also detected in the filament-rich regions. These were, however, agglomerated with the filaments, and thus they could not be successfully imaged independently of the filaments.

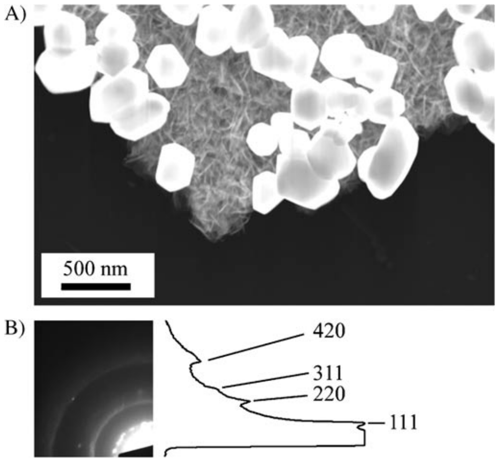

Figure 6. A) High-angle annular dark-field scanning transmission electron microscopy image showing the 200–300 nm particles and the filament-like particles present in the red-brown powder from sample **H-165**. Scale bar = 500 nm. B) Selected-area electron diffraction of an area containing only filament-like particles. The rings are indexed to *hkl* values for an *fcc* structure.

The electron diffraction pattern was collected in regions consisting of the filaments (Figure 6B). The pattern consisted of diffuse rings, which is consistent with a poorly crystallized structure. It is also worth noting that under the influence of the electron beam radiation, the probed regions showed a tendency to amorphize. The pattern appears to be consistent with an *fcc* structure, but due to the low intensity and the broadness of the rings, not all of the expected reflections were clearly visible.

Figure 7 shows the results obtained from EDXS measurements on two separate regions of **H-165**. It can clearly be determined that the 200–300 nm particles contained primarily gold (Figure 7B, spectrum ii), while the filament-like and small sphere-like particles were composed of nickel and oxygen (Figure 7B, spectrum i).

The powder X-ray diffractogram of the red-brown powder from the **H-165** sample differs from that predicted for pure $K\{Ni[Au(CN)_2]_3\}$ (Figure 8). The peaks corresponding to $K\{Ni[Au(CN)_2]_3\}$ are present, but they only account for a very small fraction of the sample. The principal pattern could be assigned either to NiO or Au, or a mixture of the two, as both are *fcc* systems with very similar lattice parameters (there is a difference of only 0.1 Å in lattice parameter *a* between Au (4.071 Å)[40] and NiO (4.178 Å)[41]).

Sample prepared at 135 °C (H-135): To further investigate the system, a reaction was also carried out at 135 °C for

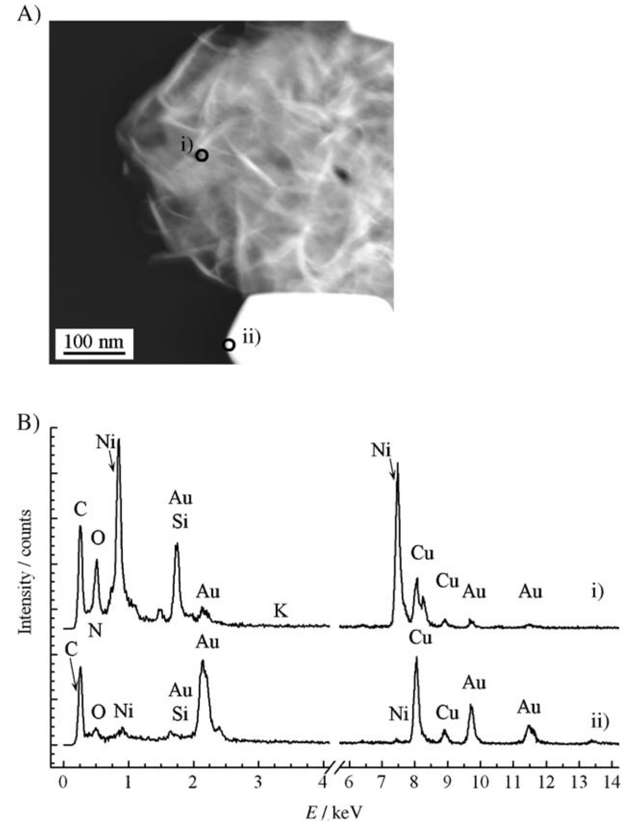

Figure 7. A) High-angle annular dark-field scanning transmission electron microscopy image of the **H-165** sample. Scale bar = 100 nm. B) Energy-dispersive X-ray spectra (EDXS) for areas highlighted in A: filament-like NiO particles (spectrum i) and Au particles (spectrum ii).

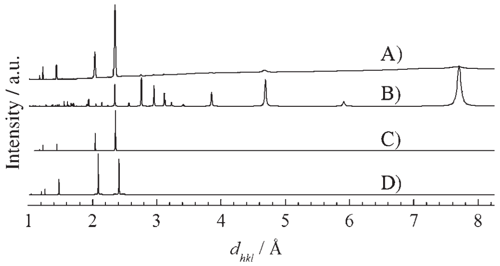

Figure 8. Comparison of the measured X-ray diffractogram of **H-165** (A) with the diffractograms predicted for K{Ni[Au(CN)$_2$]$_3$} (B), Au (C), and NiO (D).

65 h, using the same quantities of reagents. The bulk product was visually similar to **H-125**, but a small amount of red-brown powder could be observed mixed with the pale-blue powder and dark-blue crystals. This bulk product is referred to herein as **H-135**.

The same ZFC and FC magnetization experiments were also performed on sample **H-135** (Figure 5). These showed that sample **H-135** displayed magnetic behavior similar to that of **H-165**, with a maximum (at 22.5 K) and a subsidiary peak at lower temperature. The magnetization M_g at the primary peak in the ZFC measurement had a magnitude intermediate between those of the **H-125** and **H-165** samples.

Similarly to sample **H-125**, sample **H-135** was seen to be composed of a mixture of large crystal blocks and spherical nanosized particles with diameters ranging from 5 to 10 nm when investigated by TEM. The large crystals were seen to be single-crystalline by SAED, and EDXS showed that they contained carbon, nitrogen, potassium, nickel, and gold, indicative of the formula K{Ni[Au(CN)$_2$]$_3$}, as in the case of **H-125**.

Various regions of **H-135**, containing nanosized particles, were examined by EDXS. No potassium was observed in the regions containing nanoparticles. In most areas, strong signals for nickel and oxygen were seen in the EDXS spectra. Varying amounts of gold could also be observed in these regions. In some other areas, gold was the major component seen in the spectrum. The EDXS data for these different regions are shown in Figure S7. These results are consistent with the presence of various amounts of two types of nanoparticles, namely NiO and, presumably, metallic Au.

Despite the chemical difference observed by EDXS, the regions are visually very similar when observed by TEM. One difference is that in some of the nickel/oxygen-rich regions, filament-like structures similar to those observed in sample **H-165** could also be imaged, in addition to spherical particles.

Discussion

What is the chemical identity of the nanoparticles? This question can be partially addressed by examining the (S)TEM images and the EDXS and SAED data. This ensemble of data (compare, for example, the (S)TEM images of **H-125**, **H-135**, and **H-165** in Figure 4, Figure S5, and Figure 7) makes it clear that different nanoparticulate products are generated under each of the three hydrothermal temperature regimes used. However, all of the SAED data for the nanoparticle samples can be indexed to essentially the same simple *fcc* structure, which at first glance appears to suggest that the chemical composition does not change. All of the EDXS spectra in the nanoparticle regions of **H-125**, **H-135**, and **H-165** lack potassium signals and do not show a proportionate nitrogen signal for K{Ni[Au(CN)$_2$]$_3$}. Consequently, none of the examined nanoparticle products are nanocrystals of the primary K{Ni[Au(CN)$_2$]$_3$} coordination polymer.

The results obtained for the **H-165** sample clearly showed that two types of very different nanosized products were present (Figure 6): large Au particles (200–300 nm) and much smaller NiO filament-like particles, the compositions of which could clearly be identified by EDXS (Figure 7). The powder X-ray diffractogram of the bulk **H-165** sample confirms the presence of at least one of these candidates (Figure 8). Unfortunately, under our experimental conditions, X-ray diffraction methods could not discriminate between NiO and Au based on peak positions alone. Nevertheless, the relative intensities of the peaks observed between 1.0 and 2.5 Å suggest the presence of a large quantity of Au in the **H-165** sample. The presence of NiO as a minor component cannot, however, be ruled out. It must also be stressed that the NiO filaments were rather poorly crystallized, as observed by SAED, and would thus contribute less to the powder X-ray diffractogram of the **H-165** sample.

Focusing on the nanoparticles in the **H-125** sample, a strong signal for gold, as well as weaker signals for nickel and oxygen, were observed in the EDXS spectrum in all nanoparticulate regions. In light of the chemical identity of the particles observed in **H-165**, it is suggested that a mixture of Au and NiO nanoparticles is formed in the reaction at 125 °C. The structures of both NiO and Au are *fcc*,[40,41] as was the structure of the nanoparticles observed by SAED. Note that at this temperature, in contrast to the product obtained at 165 °C, the Au and NiO particles formed could not readily be distinguished on the basis of shape or size. The rather wide size distribution (2–10 nm) may have resulted from the presence of chemically different particles. Different chemical species may be expected to show different growth kinetics at a given temperature.

The EDXS data could also be interpreted as suggesting that Au_xNi_{1-x} alloy nanoparticles were formed, as opposed to the chemically segregated Au and NiO units described above. Au_xNi_{1-x} alloys have previously been reported in the literature, and their structures were also determined to be *fcc* by X-ray diffraction analyses of both bulk[42] and nanoparticle samples.[43]

The presence of pure Ni nanoparticles amongst the products of any of these high-temperature reactions is unlikely, since the reactions were carried out in water and the samples were handled in the ambient atmosphere. Indeed, it has been reported that metallic Ni nanoparticles readily oxidize in air to form Ni/NiO core–shell nanoparticles.[44] No core–shell structures were observed in any of our TEM investigations. Thus, the presence of Ni nanoparticles may be excluded.

In contrast to the **H-125** sample, the inhomogeneous chemical composition of the **H-135** nanoparticles, as determined by EDXS, is a clear indication that at least two nanoparticulate products, most probably Au and NiO, were formed under these conditions. As in the case of sample **H-125**, despite having different chemical compositions, the two types of particles could not be distinguished on the basis of shape or average diameter. In addition to the spherical particles, a few filament-like particles were present in some of the NiO-rich regions, a feature that was not observed in **H-125**, but was present to a large extent in **H-165**.

Thus, in summary, the nanoparticles produced at each of the selected temperatures (125, 135, and 165 °C) are likely to be mixtures of Au and NiO. Changes in the reaction conditions are known to affect the growth of nanoparticles, yielding different particle sizes, size distributions, and morphologies.[45] This could readily explain the differences observed between these hydrothermal samples. At lower temperatures, small, approximately spherical particles are produced. Reactions at higher temperatures (accompanied by longer reaction times) result in the growth of these particles. It is apparent that the Au and NiO particles grow in different ways. In the case of the Au nanoparticles, an Ostwald-ripening-type process results in the growth of larger particles from the dissolution of smaller particles.[46] For NiO, the aspect ratio of the particles is more affected than their diameters, yielding filament-like particles that become ever more prevalent as the reaction temperature and time are increased. The concentration of the metal ions that ultimately form the nanoparticles is also likely to be function of the reaction temperature, and is likely to affect the size and morphology of the nanoparticles.

Nanoparticle formation route: The formation of Au nanoparticles requires the reduction of Au^I ions. As no reducing agent was added to the reaction, cyanide groups most likely acted as internal reductants. Cyanide-containing coordination complexes and polymers are known to release cyanogen, $(CN)_2$, at elevated temperatures by oxidation of the cyanide groups and reduction of the metal centers.[47] In particular, cyanogels, which are amorphous Prussian Blue analogues, have been investigated for their applications as single-source precursors of binary and ternary transition metal alloys and intermetallics.[48] Superparamagnetic nanoparticle alloys of NiFe[49] and PdCo[50] have also been synthesized by the high-temperature auto-reduction of preformed cyanide-containing nanoparticles under an argon atmosphere.

Several methods for preparing NiO nanoparticles have been reported, including the thermal treatment of $Ni(OH)_2$ gels.[51] Under our experimental conditions, it is also possible that $Ni(OH)_2$ is formed as an intermediate en route to the synthesis of the observed NiO nanoparticles.

A recent report has shown that the thermal decomposition of nanoscale $Co_3[Co(CN)_6]_2$ yields Co_3O_4 nanoparticles.[52] In view of this, it may also be possible that nanoparticles of the $K\{Ni[Au(CN)_2]_3\}$ coordination polymer are formed, which decompose to yield NiO and Au nanoparticles.[53]

It is clear that the formation of nanoparticles is enhanced at higher reaction temperatures. This was evident from the successively larger contributions of the superparamagnetic impurity to the ZFC measurements (Figure 5).

Magnetic properties: The magnetic behavior observed for the **RT** sample of $K\{Ni[Au(CN)_2]_3\}$ is typical of a paramagnetic system that does not order spontaneously over the temperature range studied here (Figures 2 and 3).

The magnetic properties of the samples prepared under hydrothermal conditions show remarkable differences to the simple, paramagnetic-like behavior of the sample **RT**. The maxima observed in the ZFC measurements for the **H-125**, **H-135**, and **H-165** samples are suggestive of a superparamagnetic signature superimposed onto a paramagnetic background, as detailed below.

Superparamagnetic impurities: Superparamagnetism is a finite scale effect, and is encountered in small magnetic particles (≈20 nm diameter or less, depending on the material),[54,55] below their ordering temperature. A nanoparticle is sufficiently small that its energy is minimized when it constitutes a single magnetic domain.[56] The energy barrier KV, where K is the uniaxial anisotropy constant and V is the volume of the nanoparticle, prevents relaxation of the magnetic moment. The energy barrier is considerably reduced (compared to bulk materials) in a low-volume nanoparticle.[57] When the thermal energy is higher than the anisotropy energy barrier KV, the magnetization vector will freely fluctuate, whereas if the thermal energy is smaller, the magnetization vector will not be able to flip orientation, and hence will be in the *blocked* state. This occurs below a particular temperature called the blocking temperature T_B.

In a sample cooled in the absence of an applied magnetic field (ZFC), the magnetization vector of a nanoparticle will align itself with *its* easy axis, and the *overall* magnetization of the *sample* will be close to zero due to the random orientation of easy axes. Upon warming in an applied magnetic field, the overall magnetization will increase, as the individual magnetization vectors will align with the poling field. Upon passing through the blocking temperature T_B, the thermal energy overcomes the poling effect of the magnetic field, and randomizes the orientation of the magnetization vectors of the nanoparticles.

In an FC measurement, the magnetization vectors are oriented by the applied field upon cooling. Consequently, the measured magnetization at low temperature is high. As the temperature is increased, thermal energy randomizes the orientations of the magnetization vectors, and a decrease in magnetization is observed. Above the blocking temperature, the response is paramagnetic for both the FC and ZFC measurements.

With this in mind, an examination of the ZFC and FC magnetization measurements shown in Figure 2 (**H-125**) indicates that they contain two components: a continuously decreasing, Curie-type paramagnetic component, and a superparamagnetic component passing through its blocking temperature. The Curie-type contribution arises from the major product, $K\{Ni[Au(CN)_2]_3\}$, as is evidenced by the Curie-type magnetic behavior of the nanoparticle-free sample prepared at room temperature (Figure 2). As shown in Figure 9, the blocking temperature T_B determined for sample **H-125** under various applied fields H has an $H^{2/3}$ dependence. This behavior, which is similar to the de Almeida–Thouless law predicting the field dependence of the freezing temperature for spin-glasses,[58] has also been reported for superparamagnetic nanoparticles and is associated with the spin-glass state observed at the surface of nanoparticles.[59] Such spin-glass behavior has been observed in nanosized NiO particles.[60] This field dependency confirms that the second magnetic component is due to superparamagnetism arising from the presence of NiO nanoparticles.

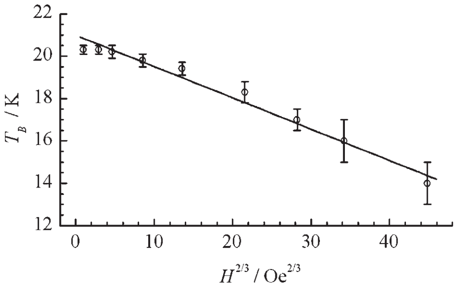

Figure 9. Field dependence of the blocking temperature T_B, determined from ZFC measurements, for sample **H-125**.

No nanoparticles could be found by TEM in the sample synthesized at room temperature, while for each hydrothermally prepared sample examined by TEM, collections of nanoscopic particles (ranging from 5 to 200 nm, depending on the sample) could readily be observed in all regions of the supporting grid (Figures 4 and 7; Figures S5 and S7). Thus, the superparamagnetic component, which is only observed in the samples prepared under hydrothermal conditions, is almost certainly due to the presence of the nanoparticles observed by TEM.

Furthermore, the shape, position, and magnitude of the maxima in the ZFC curves, which strongly depend on the temperature at which the hydrothermal reaction is carried out (Figure 5), are consistent with the formation of different products at different temperatures (as seen by TEM).

Nanoparticles obtained in the samples prepared under hydrothermal conditions, whether they consist of NiO filaments or particles, could be responsible for the observed superparamagnetic behavior. While bulk NiO is known to be an antiferromagnet ($T_N = 525$ K), NiO nanoparticles with average diameters of 3 and 7 nm have been found to be superparamagnetic, with blocking temperatures of 10 and 15 K, respectively, as determined from ZFC measurements at 100 Oe.[61] It is also worth noting that above a given nickel composition (≈50 atom % Ni), bulk Au_xNi_{1-x} alloys are ferromagnetic[62] and, more importantly, $Au_{0.45}Ni_{0.55}$ nanoparticles with an average size of 12.0 nm behave as a superparamagnetic material, with a blocking temperature of 8 K under an applied field of 500 Oe;[43] different sizes and Au:Ni ratios would certainly yield slightly different T_B values.

Recent reports have shown that nanosized gold particles display superparamagnetism[63,64] and even room temperature ferromagnetism.[65] However, this only occurs under very specific circumstances;[64,65] it is very unlikely that the observed magnetic behavior in any of our samples was due to superparamagnetic gold nanoparticles.

The presence of two peaks in the ZFC measurements for **H-135** and **H-165** (Figure 5) may be due to three different factors: size distribution, shape, and chemical identity.[54] These three effects can yield different anisotropy energy barriers, which would lead to different blocking temperatures. Thus, either the **H-135** and **H-165** samples contain two distinct superparamagnetic chemical species, or there is only one superparamagnetic species with a bimodal size distribution or different aspect ratios. In a uniaxial structure, such as a filament, an additional shape anisotropy term may also contribute to the anisotropy energy barrier.[66]

We currently have no specific control over the size, shape, or composition of the nanoparticles in these synthetic procedures. Consequently, all of the above are equally likely explanations, in theory. However, given the data described above, the two superparamagnetic species can most likely be attributed to the two differently shaped forms of NiO observed (spherical vs filament-like), which only appeared in **H-135** and **H-165**. In **H-125**, in which only NiO spherical particles were observed, only one peak was observed in the ZFC curve.

The anisotropic shape of the filament-like particles may be responsible for the increase in blocking temperature, from 20 K for the spherical particles in sample **H-125** to 22.75 K for the filament-like particles in sample **H-165**.

The field-dependent magnetization measurements for sample **H-165** at temperatures above T_B (300, 100, and 50 K) show anhysteretic behavior. This is to be expected for a sample consisting of paramagnetic and superparamagnetic species, in which the energy barrier to magnetization reversal is overcome. At 2 K (well below T_B), the loop is hysteretic and has a coercive field, consistent with the nanoparticles being in the blocked state. The same general features were observed for samples **H-135** and **H-125**: for $T > T_B$, the loops have an overall paramagnetic character, and hysteresis is observed for $T < T_B$. This is consistent with our interpretation that the ZFC/FC measurements indicate the presence of superparamagnetic species.

Shortcomings of conventional analytical methods: Clearly, the presence of even a trace amount of superparamagnetic nanoparticles can have a huge impact on the measured magnetic properties. In **H-125**, for example, a convolution of the properties of the target $K\{Ni[Au(CN)_2]_3\}$ coordination polymer and the superparamagnetic nanoparticles is observed. It must be stressed that standard characterization techniques (such as FTIR spectroscopy and elemental analysis), as well as the commonly accepted checks to ensure sample purity and identity (such as the comparison of predicted and obtained X-ray diffractograms) *failed* to uncover the presence of the nanoparticle impurity in **H-125**.

For example, samples of $K\{Ni[Au(CN)_2]_3\}$ containing up to 4.2% (by weight) of a 1:1 mixture of NiO and Au nanoparticles would still show elemental analysis results consistent with a pure sample within standard accepted tolerances. Although powder X-ray diffraction can be used as an analytical tool to quantify the composition of mixtures, the typical limit of detection for this method is about 5%, for well crystallized samples with well resolved peaks. For a nanocrystalline sample, Scherrer broadening of the linewidths tends to decrease the intensity of the reflection peaks.[67] In the case of **H-125**, in which a low concentration (below 5%) is combined with broadening, the intensity of the signal is expected to be very weak, and the presence of the nanoparticles was not detected by X-ray diffraction experiments. Also, if the impurity is poorly crystallized (as was the case for the NiO filaments formed at 165 °C), it will be harder to detect. The detection may be further complicated by the substantial peak overlap with the powder diffractogram of $K\{Ni[Au(CN)_2]_3\}$ in this case. Such small amounts of NiO and Au would also be very difficult to observe in the FTIR spectra in the 400 to 4000 cm^{-1} range. These analytical methods are therefore inappropriate for detecting low impurity levels of nanocrystalline materials.

However, such small amounts of magnetic nanoparticle impurities are more than sufficient to dominate the overall observed magnetic response. In the case of $K\{Ni[Au(CN)_2]_3\}$ presented here, comparison of the magnetic properties from samples prepared at room temperature and by hydrothermal methods suggested that a (much) closer look at the samples was imperative. However, in other cases in which the products obtained by hydrothermal methods are unique and hence inaccessible by more conventional synthetic routes (such as an analogous room temperature preparation), a comparison with "pure" samples may be difficult, if possible at all. In these cases, the danger of *erroneously* attributing the observed magnetic (or indeed any other) properties to the "pure" bulk material cannot be underestimated.

Conclusion

At room temperature, the triply-interpenetrated Prussian Blue analogue $K\{Ni[Au(CN)_2]_3\}$ can be prepared in pure form and it shows a simple Curie–Weiss-type paramagnetic behavior. Hydrothermal synthesis yielded large single crystals of $K\{Ni[Au(CN)_2]_3\}$ but also a smattering of nanoparticle impurities, which dominated the observed magnetic properties, even though conventional analytical methods were inadequate in highlighting their presence.

It should be clear that great care must be taken in the characterization of samples prepared under hydrothermal conditions. While it is obviously a highly valuable synthetic tool, especially for obtaining good quality single crystals for structural determination and by offering an alternative synthetic route for synthesizing unique materials, one must be aware that trace amounts of nanoparticulate impurities may also be generated as a result of the thermal treatment.

Observing coordination polymer samples by electron microscopy is not a common practice in the field, but in this case it was invaluable to determine the full nature of the material, thereby avoiding attribution of the magnetic properties of the sample as intrinsic properties of the $K\{Ni[Au(CN)_2]_3\}$ coordination polymer.

Although this narrative has revolved around the discussion of magnetic properties, the presence of amounts of nanoparticles small enough to be undetected by conventional analytical methods may also impact other physical properties (such as the conductivity, dielectric constant, optical, or gas adsorption properties), which are often the motivation behind the synthesis of coordination polymers. In short, such nanoscale materials often have physical properties that could inadvertently masquerade as properties of the overlying coordination polymer product. It is therefore crucial to consider this possibility when interpreting data, whether it is from the laboratory or from published literature. Finally, this work has confirmed that, given the right conditions, the hydrothermal treatment of cyanometalate polymers can generate a range of nanoparticle materials.

Experimental Section

General procedures and physical measurements: All reagents were purchased from commercial sources and were used as received without further purification. Hydrothermal reactions were carried out in sealed glass ampoules inserted into a 125 mL stainless steel reaction vessel, with 30–40 mL of H_2O placed outside of the ampoule to equalize the pressure. The vessel was heated in a Lindberg heavy-duty furnace equipped with a programmable temperature controller. The thermal profile of each reaction is specified in the synthetic description below. Infrared spectra were recorded on a Thermo Nicolet Nexus 670 FTIR spectrometer from samples prepared as pressed KBr pellets. Microanalyses (C, H, N) were performed by Mr. M. K. Yang at Simon Fraser University using a computer-controlled Carlo Erba (Model 1106) CHN analyzer.

Room temperature synthesis of K{Ni[Au(CN)$_2$]$_3$} (RT): A solution of $Ni(NO_3)_2{\cdot}6H_2O$ (29 mg, 0.10 mmol) in water (2 mL) was added to a solution of $KAu(CN)_2$ (114 mg, 0.396 mmol) in water (10 mL). A pale-green precipitate of $Ni(\mu\text{-}OH_2)_2[Au(CN)_2]_2$ formed immediately,[32] which was left stirring in the solution for 4 d. Thereafter, the precipitate had changed to a pale-blue powder, which was isolated by filtration. Its elemental analysis was found to be consistent with the chemical composition $K\{Ni[Au(CN)_2]_3\}$. This sample is referred to as **RT** herein. Yield: 72 mg (85 %); IR (KBr): $\tilde{\nu}=2170$ (s), 473 cm^{-1} (m); elemental analysis calcd for $C_6N_6Au_3NiK$: C 8.53, H 0.00, N 9.95; found: C 8.62, H trace, N 9.77.

Hydrothermal synthesis of K{Ni[Au(CN)$_2$]$_3$} (H-125): A solution of $KAu(CN)_2$ (114 mg, 0.396 mmol) in water (1 mL) was combined with a solution of $Ni(NO_3)_2{\cdot}6H_2O$ (29 mg, 0.10 mmol) in water (1 mL) in a 5 mL ampoule. Water was added to bring the total volume to ≈ 3 mL. The ampoule was sealed and loaded into the reaction vessel. The vessel was heated in a furnace from 25 to 125 °C over a period of 2 h, maintained at 125 °C for 6 h, and then slowly cooled back to 25 °C at a rate of 1 °C h^{-1}. Dark-blue hexagonal crystals of $K\{Ni[Au(CN)_2]_3\}$ (0.01–2 mm in diameter) and a pale-blue powder, also of $K\{Ni[Au(CN)_2]_3\}$, were obtained by performing the reaction under these conditions. This sample is referred to as **H-125** herein. IR: $\tilde{\nu}=2169$ (s), 473 cm^{-1} (m); elemental analysis calcd for $C_6N_6Au_3NiK$: C 8.53, H 0.00, N 9.95; found: C 8.52, H trace, N 9.96.

Using the same quantities of reagents, hydrothermal reactions were also performed at higher temperatures: 1) with a maximum of 135 °C maintained for 65 h, followed by cooling at a rate of 55 °C h^{-1} to generate sample **H-135**, and 2) a maximum temperature of 165 °C maintained for 6 h, followed by cooling at a rate of 1.4 °C h^{-1} to generate sample **H-165**.

X-ray crystallographic analysis: A blue hexagonal crystal of $K\{Ni[Au(CN)_2]_3\}$ ($0.195\times0.156\times0.074$ mm^3) was mounted on a glass fibre using epoxy adhesive. Single-crystal X-ray diffraction data, in the range $4° < 2\theta < 89.5°$, were recorded at 150 K on a Bruker SMART APEX II diffractometer equipped with a CCD area detector, a graphite monochromator, and an $Mo_{K\alpha}$ fine-focus sealed tube ($\lambda=0.71073$ Å) operated at a power of 1.5 kW (50 kV and 30 mA). The unit cell was determined to be trigonal, with space group $P312$, and unit cell parameters of $a=6.786(4)$ Å and $c=7.778(8)$ Å ($V=310.2(4)$ Å^3, $Z'=1$, $fw=844.82$, $C_6N_6Au_3NiK$, $\rho_{calcd}=4.522$). Data (5424 measured reflections, 1557 independent reflections) were corrected for absorption effects using a numerical face absorption correction (transmission range 0.0422–0.0639, $\mu=37.173$). Data reduction, including Lorentz and polarization corrections, was also performed. The structure was determined using CRYSTALS (version 12).[68] It was solved using SIR 92 and expanded through the application of Fourier techniques. All atoms were refined anisotropically. Full-matrix least-squares refinement (1309 reflections included) on F (30 parameters) converged to $R_1=0.0297$, $wR_2=0.0313$ ($I_o>2.5\sigma(I_o)$). Diagrams were generated using ORTEP-3 (version 1.076)[69] and POV-Ray (version 3.6.0).[70] Selected bond lengths and angles are reported in Table S1 in the Supporting Information. CCDC 676996 contains the supplementary crystallographic data for this paper. These data can be obtained free of charge from The Cambridge Crystallographic Data Centre via www.ccdc.cam.ac.uk/data_request/cif.

Powder X-ray diffractograms of the prepared samples were acquired on a Rigaku RAXIS-Rapid Auto diffractometer equipped with a $Cu_{K\alpha}$ source ($\lambda=1.54056$ Å) and a 0.3 mm collimator. Each sample was mounted on a glass fibre using grease and then exposed to X-rays (for 45–60 min) as the Φ axis was spun (10° s^{-1}).

Magnetometry: Magnetization measurements were performed with a Quantum Design MPMS-XL-7S SQUID magnetometer. Microcrystalline samples were packed in gelatin capsules and mounted in diamagnetic plastic straws. Direct current (DC) magnetization was measured upon cooling from 300 to 1.8 K under an applied DC field of 1 kOe. Zero-field-cooled (ZFC) and field-cooled (FC) magnetization measurements were also performed upon warming from 1.8 to 300 K under different external fields (1, 10, 50, 100, and 300 Oe). The alternating current (AC) susceptibility of all samples was also determined in zero applied DC field as a function of temperature (100 to 1.8 K). The amplitude and frequency of the AC field were 5 Oe and 10.0 Hz, respectively. The field dependence of the magnetization was determined for all samples between 20 kOe and −20 kOe at 300, 100, 50, and 2 K. All data were corrected for the diamagnetism of the constituent atoms by the use of Pascal's constants.[71]

Transmission electron microscopy and characterization: Samples were prepared by evaporating the water from an aqueous suspension of each material on a carbon-coated copper grid. Imaging was carried out using an FEI Tecnai 20 scanning transmission electron microscope (STEM) operating at 200 kV and equipped with a CCD camera. Bright-field (BF) and high-resolution (HR) images, as well as selected-area electron diffractograms (SAED), were acquired in TEM mode. High-angle annular dark-field (HAADF) imaging and energy-dispersive X-ray spectroscopy (EDXS) were carried out in STEM mode. EDXS spectra were acquired in 60 s using an EDAX unit. The images were analyzed using ImageJ software.[72]

Acknowledgements

We thank NSERC of Canada, the CFI, the BCKDF, and Simon Fraser University for financial support. We thank Dr. Li Yang for assistance with the electron microscopy experiments and Dr. Raymond J. Batchelor for assistance with the single-crystal X-ray crystallography.

---

[1] a) S. L. James, *Chem. Soc. Rev.* **2003**, *32*, 276–288; b) S. Decurtins, R. Pellaux, G. Antorrena, F. Palacio, *Coord. Chem. Rev.* **1999**, *190–192*, 841–854; c) D. J. Chesnut, D. Hagrman, P. J. Zapf, R. P. Hammond, R. J. LaDuca, R. C. Haushalter, J. Zubieta, *Coord. Chem. Rev.* **1999**, *190–192*, 737–769; d) M. Eddaoudi, D. B. Moler, H. Li, B. Chen, T. M. Reineke, M. O'Keeffe, O. M. Yaghi, *Acc. Chem. Res.* **2001**, *34*, 319–330.

[2] B. Moulton, M. J. Zaworotko, *Chem. Rev.* **2001**, *101*, 1629–1658.

[3] a) S. Kitagawa, R. Kitaura, S.-i. Noro, *Angew. Chem.* **2004**, *116*, 2388–2430; *Angew. Chem. Int. Ed.* **2004**, *43*, 2334–2375; b) H. K. Chae, D. Y. Siberio-Pérez, J. Kim, Y. Go, M. Eddaoudi, A. J. Matzger, M. O'Keeffe, O. M. Yaghi, *Nature* **2004**, *427*, 523–527; c) A. G. Wong-Foy, A. J. Matzger, O. M. Yaghi, *J. Am. Chem. Soc.* **2006**, *128*, 3494–3495; d) A. R. Millward, O. M. Yaghi, *J. Am. Chem. Soc.* **2005**, *127*, 17998–17999.

[4] J. Lefebvre, R. J. Batchelor, D. B. Leznoff, *J. Am. Chem. Soc.* **2004**, *126*, 16117–16125.

[5] a) E. J. Fernandez, J. M. Lopez-de-Luzuriaga, M. Monge, M. Montiel, M. E. Olmos, J. Perez, A. Laguna, F. Mendizabal, A. A. Mohamed, J. P. J. Fackler, *Inorg. Chem.* **2004**, *43*, 3573–3581; b) L. G.

Beauvais, M. P. Shores, J. R. Long, *J. Am. Chem. Soc.* **2000**, *122*, 2763–2772; c) M. A. Mansour, W. B. Connick, R. J. Lachicotte, H. J. Gysling, R. Eisenberg, *J. Am. Chem. Soc.* **1998**, *120*, 1329–1330; d) S. M. Drew, D. E. Janzen, C. E. Buss, D. I. MacEwan, K. M. Dublin, K. R. Mann, *J. Am. Chem. Soc.* **2001**, *123*, 8414–8415.

[6] C. Janiak, *Dalton* **2003**, 2781–2804.

[7] O. R. Evans, W. Lin, *Acc. Chem. Res.* **2002**, *35*, 511–522.

[8] a) N. D. Draper, R. J. Batchelor, B. C. Sih, Z.-G. Ye, D. B. Leznoff, *Chem. Mater.* **2003**, *15*, 1612–1616; b) C. Janiak, T. G. Scharmann, P. Albrecht, F. Marlow, R. Macdonald, *J. Am. Chem. Soc.* **1996**, *118*, 6307–6308; c) K. M. Fromm, E. D. Gueneau, J.-P. Rivera, G. Bernardinelli, H. Goesmann, *Z. Anorg. Allg. Chem.* **2002**, *628*, 171–178.

[9] a) M. J. Katz, P. M. Aguiar, R. J. Batchelor, A. A. Bokov, Z.-G. Ye, S. Kroeker, D. B. Leznoff, *J. Am. Chem. Soc.* **2006**, *128*, 3669–3676; b) M. J. Katz, H. Kaluarachchi, R. J. Batchelor, A. A. Bokov, Z.-G. Ye, D. B. Leznoff, *Angew. Chem.* **2007**, *119*, 8960–8963; *Angew. Chem. Int. Ed.* **2007**, *46*, 8804–8807.

[10] a) B. Zhao, X.-Y. Chen, P. Cheng, D.-Z. Liao, S.-P. Yan, Z.-H. Jiang, *J. Am. Chem. Soc.* **2004**, *126*, 15394–15395; b) B. D. Chandler, D. T. Cramb, G. K. H. Shimizu, *J. Am. Chem. Soc.* **2006**, *128*, 10403–10412.

[11] a) E. Coronado, P. Day, *Chem. Rev.* **2004**, *104*, 5419–5448; b) L. Ouahab, *Chem. Mater.* **1997**, *9*, 1909–1926; c) P. G. Lacroix, *Chem. Mater.* **2001**, *13*, 3495–3506; E. Coronado, J. R. Galan-Mascaros, C. J. Gomez-Garcia, V. Laukhin, *Nature* **2000**, *408*, 447–449; d) S. Bénard, P. Yu, T. Coradin, E. Rivière, K. Nakatani, R. Clément, *Adv. Mater.* **1997**, *9*, 981–984; e) Q. Ye, D.-W. Fu, H. Tian, R.-G. Xiong, P. W. H. Chan, S. D. Huang, *Inorg. Chem.* **2008**, *47*, 772–774.

[12] J. Lefebvre, D. B. Leznoff, in *Macromolecules Containing Metal and Metal-Like Elements, Vol. 5* (Eds.: A. S. Abd-El-Aziz, C. E. Carraher Jr., C. U. Pittman Jr., M. Zeldin), Wiley-Interscience, **2005**, pp. 155–208.

[13] Special issue on molecule-based magnetism: *Polyhedron* **2007**, *26*.

[14] F. Herren, P. Fisher, A. Ludi, *Inorg. Chem.* **1980**, *19*, 956–959.

[15] a) M. Verdaguer, A. Bleuzen, V. Marvaud, J. Vaissermann, M. Seuleiman, C. Desplanches, A. Scuiller, C. Train, R. Garde, G. Gelly, C. Lomenech, I. Rosenman, P. Veillet, C. Cartier, F. Villain, *Coord. Chem. Rev.* **1999**, *190–192*, 1023–1047; b) M. Verdaguer, G. S. Girolami, in *Magnetism: Molecules to Materials V, Vol. 5* (Eds.: J. S. Miller, M. Drillon), Wiley-VCH, Weinheim, **2005**, pp. 283–346.

[16] a) Ø. Hatlevik, W. E. Buschmann, J. Zhang, J. L. Manson, J. S. Miller, *Adv. Mater.* **1999**, *11*, 914–918; b) S. M. Holmes, G. S. Girolami, *J. Am. Chem. Soc.* **1999**, *121*, 5593–5594.

[17] O. Sato, T. Iyoda, A. Fujishima, K. Hashimoto, *Science* **1996**, *272*, 704.

[18] S. Bonhommeau, G. Molnár, A. Galet, A. Zwick, J.-A. Real, J. J. McGarvey, A. Bousseksou, *Angew. Chem.* **2005**, *117*, 4137–4141; *Angew. Chem. Int. Ed.* **2005**, *44*, 4069–4073.

[19] a) I. V. Markov, *Crystal Growth for Beginners: Fundamentals of Nucleation, Crystal Growth, and Epitaxy*, World Scientific, New Jersey, **1995**; b) J. Hulliger, *Angew. Chem.* **1994**, *106*, 151–171; *Angew. Chem. Int. Ed. Engl.* **1994**, *33*, 143–162.

[20] O. M. Yaghi, G. Li, H. Li, *Chem. Mater.* **1997**, *9*, 1074–1076.

[21] P. Batail, K. Boubekeur, M. Fourmigué, J.-C. P. Gabriel, *Chem. Mater.* **1998**, *10*, 3005–3015.

[22] a) G. Demazeau, *J. Mater. Chem.* **1999**, *9*, 15–18; b) K. Byrappa, M. Yoshimura, *Handbook of Hydrothermal Technology: Technology for Crystal Growth and Materials Processing*, Noyes Publications, New Jersey, USA, **2001**.

[23] J. Bernstein, R. J. Davey, J.-O. Henck, *Angew. Chem.* **1999**, *111*, 3646–3669; *Angew. Chem. Int. Ed.* **1999**, *38*, 3440–3461.

[24] R. H. Laye, E. J. L. McInnes, *Eur. J. Inorg. Chem.* **2004**, 2811–2818.

[25] S. Feng, R. Xu, *Acc. Chem. Res.* **2001**, *34*, 239–247.

[26] C. S. Cundy, P. A. Cox, *Chem. Rev.* **2003**, *103*, 663–702.

[27] a) R. Murugavel, M. G. Walawalkar, M. Dan, H. W. Roesky, C. N. R. Rao, *Acc. Chem. Res.* **2004**, *37*, 763–774; b) J. Livage, *Coord. Chem. Rev.* **1998**, *178–180*, 999–1018.

[28] a) A. K. Cheetham, C. N. R. Rao, R. K. Feller, *Chem. Commun.* **2006**, 4780–4795; b) J. Y. Lu, *Coord. Chem. Rev.* **2003**, *246*, 327–347; c) S. B. Artemkina, N. G. Naumov, A. V. Virovets, V. E. Fedorov, *Eur. J. Inorg. Chem.* **2005**, 142–146.

[29] a) B. L. Cushing, V. L. Kolesnichenko, C. J. O'Connor, *Chem. Rev.* **2004**, *104*, 3893–3946; b) M. Rajamathi, R. Seshadri, *Curr. Opin. Solid State Mater. Sci.* **2002**, *6*, 337–345.

[30] a) X.-M. Chen, M.-L. Tong, *Acc. Chem. Res.* **2007**, *40*, 162–170; b) X.-M. Zhang, *Coord. Chem. Rev.* **2005**, *249*, 1201–1219.

[31] a) D. B. Leznoff, B.-Y. Xue, B. O. Patrick, V. Sanchez, R. C. Thompson, *Chem. Commun.* **2001**, 259–260; b) D. B. Leznoff, B.-Y. Xue, C. L. Stevens, A. Storr, R. C. Thompson, B. O. Patrick, *Polyhedron* **2001**, *20*, 1247–1254; c) D. B. Leznoff, B.-Y. Xue, R. J. Batchelor, F. W. B. Einstein, B. O. Patrick, *Inorg. Chem.* **2001**, *40*, 6026–6034; d) C. J. Shorrock, B.-Y. Xue, P. B. Kim, R. J. Batchelor, B. O. Patrick, D. B. Leznoff, *Inorg. Chem.* **2002**, *41*, 6743–6753; e) L. Ouyang, P. M. Aguiar, R. J. Batchelor, S. Kroeker, D. B. Leznoff, *Chem. Commun.* **2006**, 744–746.

[32] J. Lefebvre, F. Callaghan, M. J. Katz, J. E. Sonier, D. B. Leznoff, *Chem. Eur. J.* **2006**, *12*, 6748–6761.

[33] K. R. Dunbar, R. A. Heintz, *Prog. Inorg. Chem.* **1997**, *45*, 283–391.

[34] S. C. Abrahams, J. L. Bernstein, R. Liminga, *J. Chem. Phys.* **1980**, *73*, 4585–4590.

[35] W. Dong, L.-N. Zhu, Y.-Q. Sun, M. Liang, Z.-Q. Liu, D.-Z. Liao, Z.-H. Jiang, S.-P. Yan, P. Cheng, *Chem. Commun.* **2003**, 2544–2545.

[36] W. Dong, Q.-L. Wang, S.-F. Si, D.-Z. Liao, Z.-H. Jiang, S.-P. Yan, P. Cheng, *Inorg. Chem. Commun.* **2003**, *6*, 873–876.

[37] R. L. Carlin, *Magnetochemistry*, Springer, Berlin (Germany), **1986**.

[38] J. Lefebvre, D. Chartrand, D. B. Leznoff, *Polyhedron* **2007**, *26*, 2189–2199.

[39] AC-susceptibility measurements were also made on samples **RT** and **H-125** (Figure S4). The AC measurements are consistent with the DC measurements presented above. In particular, no signal in the χ'' was observed for **RT**, while a maximum in χ'' at 20.5 K was observed for **H-125**. The temperature dependence of the AC susceptibility of the **H-125** sample was also found to be frequency-dependent (Figure S4B).

[40] E. R. Jette, F. Foote, *J. Chem. Phys.* **1935**, *3*, 605–616.

[41] S. Sasaki, K. Fujino, Y. Takeuchi, *P. Jpn. Acad. B Phys.* **1979**, *55*, 43–48.

[42] M. Bienzle, T. Oishi, F. Sommer, *J. Alloys Compd.* **1995**, *220*, 182–188.

[43] R. Brayner, T. Coradin, M.-J. Vaulay, C. Mangeney, J. Livage, F. Fiévet, *Colloids Surf. A* **2005**, *256*, 191–197.

[44] B. Rellinghaus, S. Stappert, E. F. Wassermann, H. Sauer, B. Spliethо, *Eur. Phys. J. D* **2001**, *16*, 249–252.

[45] Y.-w. Jun, J.-H. Lee, J.-s. Choi, J. Cheon, *J. Phys. Chem. B* **2005**, *109*, 14795–14806.

[46] a) E. Matijeviec, *Chem. Mater.* **1993**, *5*, 412–426; b) D. V. Talapin, A. L. Rogach, M. Haase, H. Weller, *J. Phys. Chem. B* **2001**, *105*, 12278–12285; c) M. B. Mohamed, Z. L. Wang, M. A. El-Sayed, *J. Phys. Chem. A* **1999**, *103*, 10255–10259; d) C. B. Murray, C. R. Kagan, M. G. Bawendi, *Annu. Rev. Mater. Sci.* **2000**, *30*, 545–610.

[47] a) J. Chomic, J. Cernak, *Thermochim. Acta* **1985**, *93*, 93; b) P. K. Gallagher, J. P. Luongo, *Thermochim. Acta* **1975**, *12*, 159–164.

[48] M. Vondrova, C. M. Burgess, A. B. Bocarsly, *Chem. Mater.* **2007**, *19*, 2203–2212.

[49] B. Folch, J. Larionova, Y. Guari, L. Datas, C. Guérin, *J. Mater. Chem.* **2006**, *16*, 4435–4442.

[50] M. Vondrova, T. Klimczuk, V. L. Miller, B. W. Kirby, N. Yao, R. J. Cava, A. B. Bocarsly, *Chem. Mater.* **2005**, *17*, 6216–6218.

[51] a) C. L. Carnes, J. Stipp, K. J. Klabunde, *Langmuir* **2002**, *18*, 1352–1359; b) S. A. Makhlouf, F. T. Parker, F. E. Spada, A. E. Berkowitz, *J. Appl. Phys.* **1997**, *81*, 5561–5563.

[52] D. H. M. Buchold, C. Feldmann, *Chem. Mater.* **2007**, *19*, 3376–3380.

[53] The hydrothermal reactions reported here used $Ni(NO_3)_2{\cdot}6H_2O$ and $KAu(CN)_2$ as starting materials. We also performed control experiments, which showed that superparamagnetic nanoparticle impurities were obtained when preformed, bulk $K\{Ni[Au(CN)_2]_3\}$ (**RT**) was used as a precursor.

[54] a) C. P. Bean, J. D. Livingston, *J. Appl. Phys.* **1959**, *30*, S120–S129; b) S. Trudel, R. H. Hill, *Polyhedron* **2007**, *26*, 1863–1870.

[55] S. Trudel, C. H. W. Jones, R. H. Hill, *J. Mater. Chem.* **2007**, *17*, 2206–2218.

[56] C. Kittel, *Phys. Rev.* **1946**, *70*, 965–971.

[57] E. C. Stoner, E. P. Wohlfarth, *Philos. Trans. R. Soc. London, A* **1948**, *240*, 599.

[58] J. R. L. de Almeida, D. J. Thouless, *J. Phys. A* **1978**, *11*, 983–990.

[59] a) X. Batlle, A. Labarta, *J. Phys. D* **2002**, *35*, R15–R42; b) R. W. Chantrell, M. El-Hilo, K. O'Grady, *IEEE Trans. Magn.* **1991**, *27*, 3570–3578.

[60] a) J. B. Yi, J. Ding, Y. P. Feng, G. W. Peng, G. M. Chow, Y. Kawazoe, B. H. Liu, J. H. Yin, S. Thongmee, *Phys. Rev. B* **2007**, *76*, 224402; b) R. H. Kodama, S. A. Makhlouf, A. E. Berkowitz, *Phys. Rev. Lett.* **1997**, *79*, 1393–1396.

[61] M. Ghosh, K. Biswas, A. Sundaresan, C. N. R. Rao, *J. Mater. Chem.* **2006**, *16*, 106–111.

[62] a) R. Kuentzler, J. P. Kappler, *J. Phys. F* **1979**, *9*, 195–206; b) A. R. Kaufman, S. T. Pan, J. R. Clark, *Rev. Mod. Phys.* **1945**, *17*, 87–92.

[63] H. Hori, T. Teranishi, M. Taki, S. Yamada, M. Miyake, Y. Yamamoto, *J. Magn. Magn. Mater.* **2001**, *226–230*, 1910–1911.

[64] P. Dutta, S. Pal, M. S. Seehra, M. Anand, C. B. Roberts, *Appl. Phys. Lett.* **2007**, *90*, 213102.

[65] P. Crespo, R. Litrán, T. C. Rojas, M. Multigner, J. M. de la Fuente, J. C. Sánchez-López, M. A. García, A. Hernando, S. Penadés, A. Fernández, *Phys. Rev. Lett.* **2004**, *93*, 087204.

[66] a) J. L. Dormann, L. Bessais, D. Fiorani, *J. Phys. C Solid State Phys.* **1988**, *21*, 2015–2034; b) F. Dumestre, B. Chaudret, C. Amiens, M.-C. Fromen, M.-J. Casanove, P. Renaud, P. Zurcher, *Angew. Chem.* **2002**, *114*, 4462–4465; *Angew. Chem. Int. Ed.* **2002**, *41*, 4286–4289.

[67] P. Scherrer, in *Kolloidchemie*, 3rd edition, 1920 edition (Ed.: R. Zsigmondy), **1918**, p. 394.

[68] P. W. Betteridge, J. R. Carruthers, R. I. Cooper, K. Prout, D. J. Watkin, *J. Appl. Crystallogr.* **2003**, *36*, 1487.

[69] L. J. Farrugia, *J. Appl. Crystallogr.* **1997**, *30*, 565.

[70] T. D. Fenn, D. Ringe, G. A. Petsko, *J. Appl. Crystallogr.* **2003**, *36*, 944–947.

[71] O. Kahn, *Molecular Magnetism*, VCH, Weinheim, **1993**.

[72] M. D. Abramoff, P. J. Magelhaes, S. J. Ram, *Biophotonics International* **2004**, *11*, 36–42.

Received: February 12, 2008